European Polymer Journal 198 (2023) 112410

Contents lists available at ScienceDirect

European Polymer Journal

journal homepage: www.elsevier.com/locate/europolj

Shedding light on the microstructural differences of polymer latexes synthesized from bio-based and oil-based C8 acrylate isomers

Shaghayegh Hamzehlou [a,*], Aitor Barquero [a,*], Amaia Agirre [a], Fernando Ruipérez [b], Jose Ramon Leiza [a]

[a] POLYMAT and Applied Chemistry Department, Faculty of Chemistry, University of the Basque Country UPV/EHU, Joxe Mari Korta Center, 20018 Donostia-San Sebastián, Spain

[b] POLYMAT and Physical Chemistry Department, Faculty of Pharmacy, University of the Basque Country UPV/EHU, 01006 Vitoria-Gasteiz, Spain

ARTICLE INFO

Keywords:
Emulsion polymerization
Monte Carlo simulation
Bio-based acrylate monomers
Polymer microstructure
DFT calculations

ABSTRACT

There is a great interest in replacing traditional oil-based monomers with more renewable bio-based ones. However, their replacement in current formulations is not straightforward. Herein, we investigate the origin of the microstructural differences of the homopolymers of 2-octyl acrylate (2-OA, bio-based) and its isomer 2-ethylhexyl acrylate (2-EHA, oil-based) synthesized by emulsion polymerization through Density Functional Theory calculations (DFT) and a kinetic Monte Carlo study. DFT calculations show that hydrogen abstraction from the polymer backbone in 2-EHA homopolymer is predominant comparing to the chain transfer to polymer reaction in the side chain, while this trend is inverse for 2-OA homopolymer. The Monte Carlo model is able to fit well the experimental data of both homopolymerizations, and predicts the microstructural differences between the two systems, namely; higher amount of gel and molar mass of the gel in 2-OA homopolymerization.

1. Introduction

Climate change and depletion of natural resources are the driving forces for the development of more sustainable solutions in the production of polymeric materials. For instance, in the coating and adhesive industry, there has been a shift from solvent-borne to water-borne products to reduce the emission of volatile organic compounds. This has led to the development of techniques such as emulsion polymerization in industrial scale. Yet, there is still the challenge of transitioning from the traditional petroleum based monomers to the more sustainable and renewable bio-based ones [1].

There are many sources of bio-based monomers. Plant oils, terpenes, carbohydrates and lignin derivatives are among the most abundant sources for bio-based molecules that can be chemically transformed to produce monomers [2]. A very common method to produce bio monomers is to separately obtain a bio-based unsaturated acid and a bio based alcohol, and then carry out an esterification reaction to obtain the monomer. Like this, some monomer families such as itaconates, maleates, fumarates or crotonates can be produced 100 % from renewable sources [3–5]. However, using these monomers can be a great challenge, as more often than not, their low propagation rates and unfavorable reactivity ratios with other monomers make them not suitable to produce the desired polymers [6]. Acrylates and methacrylates on the other hand offer great reactivity, but they are not easy to obtain completely from bio-based sources. Acrylic and methacrylic acid can be completely produced from biomass in lab scale [7,8], but they are still no readily available in commercial scale, so in most cases the petroleum-based acids are used instead. Thus, partially bio-based acrylates and methacrylates (produced from oil-based (meth)acrylic acid and a bio-based alcohol) can offer an acceptable compromise between their bio-content and their availability and industrial applicability (at least until the bio-sourced routes are commercially available).

Within this strategy, 2-octyl acrylate (2-OA) is a promising candidate to be used in the production of (partially) bio-based adhesives and coatings [9–11]. The production of this monomer via (trans)esterification of acrylic acid (or derivative esters) with bio-based 2-octanol has already been industrialized and commercialized [12,13], and the final monomer has around 73% of bio-sourced carbon. Structurally, it is an isomer of the widely used commercial oil-based monomer 2-ethylhexyl acrylate (2-EHA) and the only difference between their structure lies on the position and length of the branch on the ester, as showed in Fig. 1.

Due to their structural similarity, it could be tempting to assume that

* Corresponding authors.
E-mail addresses: shaghayegh.hamzehlou@ehu.eus (S. Hamzehlou), aitor.barquero@ehu.eus (A. Barquero).

https://doi.org/10.1016/j.eurpolymj.2023.112410
Received 28 June 2023; Received in revised form 23 August 2023; Accepted 3 September 2023
Available online 9 September 2023

their behavior during the polymerization would be the same. However, Badía *et al.* showed that there are significant differences on the microstructure of the pressure sensitive adhesives formulated with bio-based 2-OA instead of 2-EHA [9]. The pressure sensitive adhesives (PSA) in the mentioned work were synthesized by semibatch emulsion polymerization at 70 °C in which bio-based monomers 2-OA and isobornyl methacrylate replaced a typical formulation of the PSA (2EHA:MMA:AA (84:15:1 wt%)). They reported a higher gel fraction (degree of crosslinking) and soluble molar mass in the bio-based system, which forced them to use chain transfer agents to control the microstructure. Later, Barrenetxe *et al.* did a more systematic comparison between the emulsion homopolymerization of these two monomers, as well as with their methacrylic equivalents [14]. They observed that despite the similar overall polymerization kinetics (in terms of conversion), the final microstructure was different. Once again, they found that the gel fraction was higher for 2-OA, but not only that, the molar mass corresponding to this population was higher too. Interestingly, the total degree of branching (calculated quantifying the quaternary carbon by ^{13}C NMR) was higher for 2-EHA.

All the microstructural differences were attributed to chain transfer to polymer reactions (inter and intramolecular). Acrylates are known for having intra and intermolecular hydrogen abstraction on the main chain [15–17], which can lead to short and long chain branching and crosslinking points in the polymer. However, these two monomers each have an additional labile hydrogen in the methine (CH) group on the side chain after polymerization (see Fig. 1), that can also be abstracted by intermolecular chain transfer to polymer reaction. The authors argued that this hydrogen should be more labile in 2-OA compared to 2-EHA, because it is closer to the oxygen, and that this explains that both the gel fraction and molar mass of the gel are higher for 2-OA homopolymer.

In this work, we assess the above hypothesis on the origin of the microstructural differences between 2-EHA and 2-OA using Density Functional Theory (DFT) calculations. The activation energy of hydrogen abstractions by intermolecular chain transfer to polymer reactions in the polymer backbone and side chains of the homopolymers of 2-OA and 2-EHA as well as the ratio between the corresponding rate coefficients were calculated. In light of the DFT results, a Monte Carlo model for seeded semibatch emulsion polymerization was used to fit the experimental data. Modeling these two monomers is challenging, as there is a notable lack of reported rate coefficients for most of the reactions. Therefore, in this approach we borrow some of the missing rate coefficients from similar monomers such as n-butyl acrylate and estimate the most sensitive parameters to fit the kinetics, branching density and complete molar mass distribution of the polymer. Note that herein we do not intend to report accurate values for the estimated kinetic parameters, but to explain the origin of the microstructural differences between these two similar monomers.

2. Synthesis and characterization of the latexes

The experimental data of the homopolymerizations of 2-EHA and 2-OA by seeded emulsion polymerization was obtained from ref 14 (see Supporting Information section S.1 for a summarized description). Here, briefly the polymerization conditions and characterization methods are described. For more details, the reader is referred to the mentioned work.

The polymerizations were carried out at 70 °C by seeded semibatch emulsion polymerization. The seed was made of polystyrene (81 nm), to avoid chain transfer to the seed polymer chains. A thermal water-soluble initiator (potassium persulfate, KPS) was used to initiate the polymerization. The acrylate monomer was fed to the reactor during 3 h and an additional hour of postpolymerization was allowed. The latexes had a final solids content of 30% and particle sizes of around 250 nm. During the polymerization, small aliquots (2–3 mL) were withdrawn for characterization.

Conversion was calculated from measuring the unreacted monomer by gas chromatography. Z-average particle size diameters were measured by Dynamic Light Scattering. The branching density (BD, defined as the number of quaternary carbons to nonbranched carbons) was measured by quantifying the percentage of quaternary carbon by solid-state ^{13}C NMR following previously reported procedures [18–20]. It was calculated as the ratio between the quaternary carbon at 48 ppm to the methyl peak at 13 ppm (see Equation 1) and the standard deviation (SD) of the measurement was calculated as reported by Castignolles *et al.* using equation 2 [19].

$$BD = \frac{I(C_q)}{I(C_{CH_3})} \times 100 \tag{1}$$

$$SD(\%) = \frac{100}{SNR}\sqrt{\frac{\Delta f_q{}^2 I(C_{CH_3})^2 + \Delta f_{CH_3}{}^2 I(C_q)^2}{\Delta f_q{}^2 I(C_{CH_3})^2}} \tag{2}$$

where $I(C_q)$ refers to the integral of the quaternary carbon peak, $I(C_{CH3})$ refers to the integration of the methyl peak in the side chain, SNR is the signal-to-noise ratio and Δf_q and Δf_{CH3} are the width of the spectral range of $I(C_q)$ and $I(C_{CH3})$, respectively. The signal-to-noise ratio was calculated using the SNR calculation script in MestReNova (v. 11.0.4–18998) using the region between 200 and 220 ppm for the baseline.

Absolute molar mass of the complete molar mass distributions were measured by Asymmetric-Flow Field-Flow Fractionation (AF4) in combination with Multi Angle Light Scattering (MALS) and Refractive Index (RI) detectors (all from Wyatt Technology, Santa Barbara, CA). The gel content was measured by two methods: soxhlet extraction and from the Refractive Index chromatogram of the AF4 measurements. Soxhlet extraction was carried out for 24 h using THF in reflux as solvent and the gel fraction was calculated gravimetrically and defined as the nonsoluble fraction [15,16]. In the AF4 method, the gel was measured by integrating the area of the Refractive Index chromatogram of the sol (low molar mass mode) and gel (high molar mass mode) fractions and calculating their relative weight. The criterion to choose the integration limits was that all polymer with weight average molar mass ($\overline{M_w}$) higher

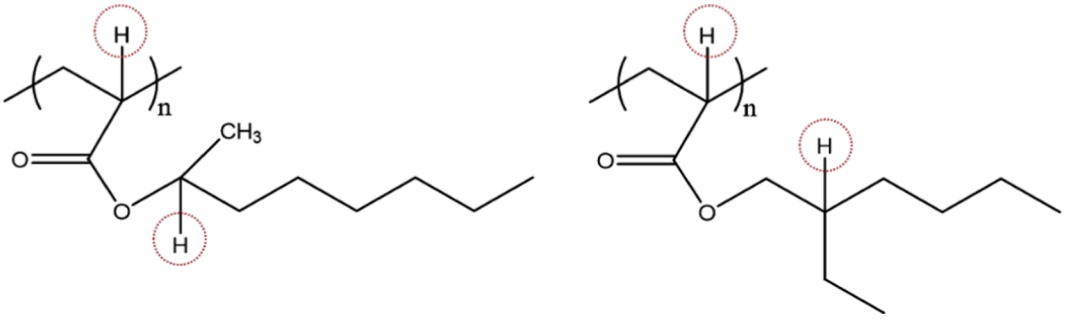

Fig. 1. Chemical structure of poly(2-octyl acrylate) (left) and poly(2-ethylhexyl acrylate) (right) with marked labile H atoms.

than 10^8 g mol^{-1} was considered gel. This criterion was selected so the results could be compared to gel fraction in the Monte Carlo model, which considers the high molar mass modality of the full molar mass distribution as gel which is equivalent of considering the limit of 10^8 g mol^{-1}.A detailed example of the calculation of the gel content by the AF4/MALS/RI data is explained in section S.2 of the Supporting Information (SI).

3. Monte Carlo model of the seeded semibatch emulsion homopolymerizations of 2-OA or 2-EHA

Several works have shown the use of Monte Carlo models to simulate the (semi)batch (mini)emulsion polymerization in different systems considering mono [21–25] or polydispersed particle size distribution [26,27]. Herein, Monte Carlo (MC) simulations previously reported [25] for miniemulsion polymerization were upgraded and used for the seeded semibatch emulsion polymerization. Here, we present a brief explanation of the important aspects of the simulation, for more details the reader is referred to the mentioned reference. The kinetic Monte Carlo algorithm proposed by Gillespie [28] was implemented in the model in which the experimental rate coefficients are transformed into stochastical rate coefficients using a control volume and Avogadrós number. The propensity of each reaction is its rate. The probability of each reaction is defined as its rate over the sum of all reaction rates. Using random numbers and the probabilities, the next reaction and time interval between two reactions are calculated. In this simulation approach, the initial control volume is defined by the seed particle volume (a monodisperse seed latex and no secondary nucleation is considered in the model, the later assumption is supported by the experimental evolution of the number of particles through the reaction, see Figure S.4) and the growth of the seed particles during the semibatch emulsion polymerization was accounted in the model. One particle with its corresponding water phase is considered in the simulations. The solids content defines the control volume of the water phase. The control volume of the water phase and organic phase updates at each time interval according to the feeding rates. Each particle exchanges matter with its own water phase. Monomer partitioning was calculated using partition coefficients, which are considered constant trough the reaction. The model accounts for reactions in both aqueous and particle phases, entry and exit of radicals were considered as well as calculation of the average number of the radicals per particle, in each simulation only one particle with its water phase was simulated. Radical entry was considered to occur by diffusion of surface active oligoradicals and by precipitation of oligoradicals when they become insoluble. Molar solubility of all species in the aqueous phase was followed using the approach proposed by Zubitur *et al.* [29] as described in reference [25]. In order to get results with statistical meaning, the simulation were repeated 20 times, which is equivalent of simulating 20 particles. The model was coded in Fortran under Linux and simulation of each particles takes about 5–6 h in a PC with 16 cores Intel(R) Xeon(R) CPU E5620 @2.40 GHZ. A more detailed description of the kinetic scheme, parameters and kinetic coefficients is presented in section S.3 of the Supporting Information.

4. Details of the DFT calculations

The usefulness of quantum chemistry in the determination of reaction kinetics in radical polymerizations has been previously established [30–34].

In this work, all geometry optimizations were carried out within density functional theory (DFT) using the M062X functional [35] combined with the 6–31 + G(d) basis set [36] in gas phase. To confirm that the optimized structures were minima or transition states on the potential energy surfaces, frequency calculations were carried out at the same level of theory. These frequencies were then used to evaluate the zero-point vibrational energy (ZPVE) and the thermal corrections, at T = 343.15 K, in the harmonic oscillator approximation. Single-point calculations using the 6–311++G(2df,2p) basis set [37] were performed on the optimized structures in order to refine the electronic energy. All the calculations were performed with the Gaussian 16 suite of programs [38]. The molecular models used in the simulations consist of one monomer unit. The kinetic rate coefficient was calculated with the Eyring equation from transition state theory [39,40] (Eq. (3)):

$$k(t) = \kappa(T)\frac{k_b T}{h}\left(c^0\right)^{1-m}\exp\left[-\frac{\Delta G^{\ddagger}}{RT}\right] \quad (3)$$

where T is the absolute temperature, R is the universal gas constant, k_b is the Boltzmann constant, h is the Plancḱs constant, $c^0 (= \frac{PR}{T})$ is the standard unit of concentration, m is the molecularity of the reaction, $\Delta G^{\ddagger}$ is the Gibbs free energy of the activation and $\kappa(T)$ is the tunnelling correction factor defined by Eq. (4):

$$\kappa(T) = 1 + \frac{1}{24}\left(\frac{hc\nu^{\ddagger}}{k_b T}\right)^2\left(1 + \frac{RT}{\Delta E_0}\right) \quad (4)$$

where $\nu^{\ddagger}$ is the imaginary frequency in the transition state and ΔE_0 is the electronic barrier height.

5. Results and discussion

5.1. DFT calculations

Fig. 2 presents the intermolecular chain transfer reaction mechanisms simulated for the homopolymerization of 2-OA and 2-EHA with the model molecules. For each monomer, 2 scenarios of the intermolecular chain transfer to polymer were considered: the abstraction of the hydrogen from the polymer backbone (referred as k_{tr1}^{pol}) and the second one which is the abstraction of the hydrogen from the side chain (referred as k_{tr2}^{pol}). The polymer chain in the molecular models for the DFT calculations were substituted by a methyl group.

Fig. 3 shows the potential surface energy (PES) of the two possible hydrogen abstraction reactions in 2-OA (Fig. 3**a**) and 2-EHA (Fig. 3**b**) homopolymerizations. Starting from the isolated reactants, the first step is the formation of a complex and then the hydrogen abstraction reaction goes through transition state (TS) to generate a tertiary radical (Intermediate). It can be seen that the barrier of the TS is very similar in both cases of hydrogen abstraction of 2-OA homopolymerization, i.e. 23.67 kcal/mol and 23.36 kcal/mol for the hydrogen abstraction from the main backbone and side chain, respectively. However, the intermediate of the hydrogen abstraction from the chain backbone shows to be more stable (3.05 kcal/mol for k_{tr1}^{pol} compared to 12.06 kcal/mol for k_{tr2}^{pol}). In order to calculate the activation energy comparable to the experimental activation energy of the reaction, it is preferred to use the electronic barrier height, instead of the Gibbs free energy. The electronic barrier for k_{tr1}^{pol} is calculated as $\Delta E_0 = 9.32$ kcal/mol (39.0 kJ/mol) which is lower than the value calculated for k_{tr2}^{pol} $\Delta E_0 = 11.27$ kcal/mol (47.13 kJ/mol).

Using the Gibbs free energy of the barrier of the transition states, the rate coefficients were calculated for each possible reaction. The absolute values of the rate coefficients are presented in the Supporting Information (Table S.3 in section S.4). As the absolute values are highly dependent on the level of theory used in the calculations, the relative values were used as guide in this work rather than using the calculated rate coefficients by DFT. Despite higher electronic barrier for the hydrogen abstraction from the side chains of the polymer, the entropic contribution let to higher rate coefficient of this reaction compared to the hydrogen abstraction from the backbone polymer chain. The ratio of the calculated chain transfer to polymer coefficients is:$\mathbf{k_{tr1}^{pol}/k_{tr2}^{pol}} = 0.68$, which shows that the abstraction of the hydrogen from the side chain is more favourable in the case of 2-OA polymerization.

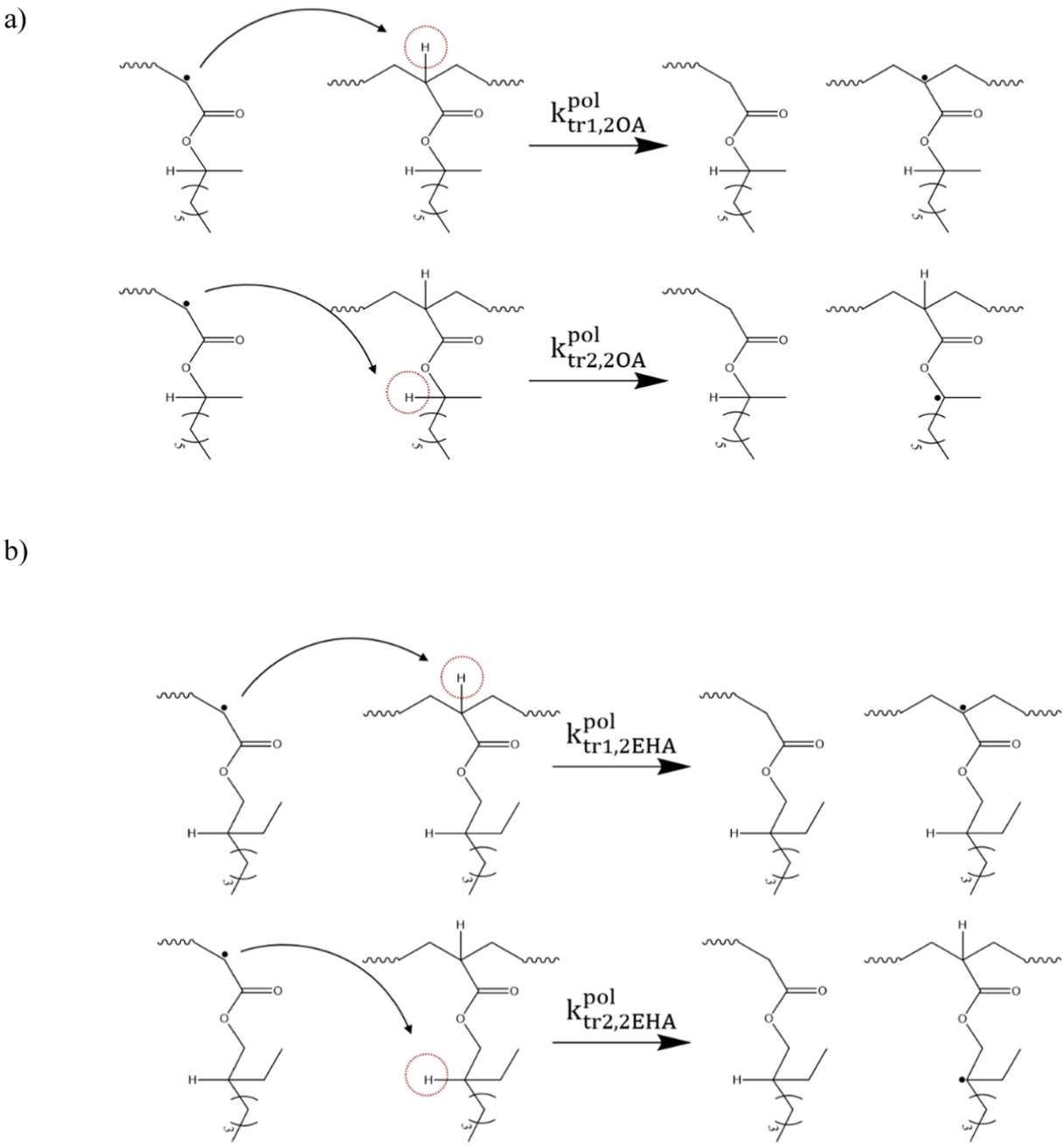

Fig. 2. Possible reaction mechanisms of intermolecular chain transfer to polymer reaction in homopolymerizations of a) 2-OA and b) 2-EHA.

The same analysis has been done for 2-EHA intermolecular chain transfer to polymer. It can be seen that the barrier of the TS are 26.27 kcal/mol and 27.35 kcal/mol for k^{pol}_{tr1} and k^{pol}_{tr2}, respectively, showing slightly higher barrier in Gibbs free energy for the transition state of k^{pol}_{tr2}. The same trend is observed for the electronic barriers calculated for 2-EHA, showing higher activation energy for k^{pol}_{tr2} ($\Delta E_0 = 12.06$ kcal/mol (50.45 kJ/mol)) compared to k^{pol}_{tr1} ($\Delta E_0 = 9.22$ kcal/mol (38.55 kJ/mol)) although with higher difference. The ratio of the calculated chain transfer to polymer coefficients shows that the transfer to polymer from the chain backbone is more favourable ($k^{pol}_{tr1}/k^{pol}_{tr2} = 5.32$) in the case of 2-EHA (see absolute values in Table S.3).

Both k^{pol}_{tr1} and k^{pol}_{tr2} show higher activation energies in 2-EHA compared with 2-OA. In addition, the overall rate coefficient of intermolecular chain transfer to polymer ($k^{pol}_{tr} = k^{pol}_{tr1} + k^{pol}_{tr2}$) for 2-OA shows higher values than 2-EHA ($k^{pol}_{tr,2OA} > k^{pol}_{tr,2EHA}$). These findings are in line with the reported experimental results showing higher gel content for 2-OA.

Having two abstractable hydrogens in both monomers can affect the overall chain transfer to monomer rate coefficient compared to other acrylate monomers with only one abstractable hydrogen such as n-butyl acrylate. To the best of our knowledge, there is no data available on the chain transfer to monomer coefficient of 2-EHA, however in the literature the experimental data on the molar mass of 2-EHA was well represented using the chain transfer to monomer of n-butyl acrylate [41]. In the case of 2-OA, there is a complete lack of kinetic data as it is relatively new monomer. Herein, we study the two possible reaction paths of chain transfer to monomer in 2-OA by DFT calculations. Fig. 4 shows the reaction routes simulated. The polymer chains in the molecular models for the DFT calculations were substituted by a methyl group.

Fig. 5 shows the potential surface energy of two reaction paths of transfer to monomer in 2-OA. Starting from reactants, the reaction goes

a) 2-OA

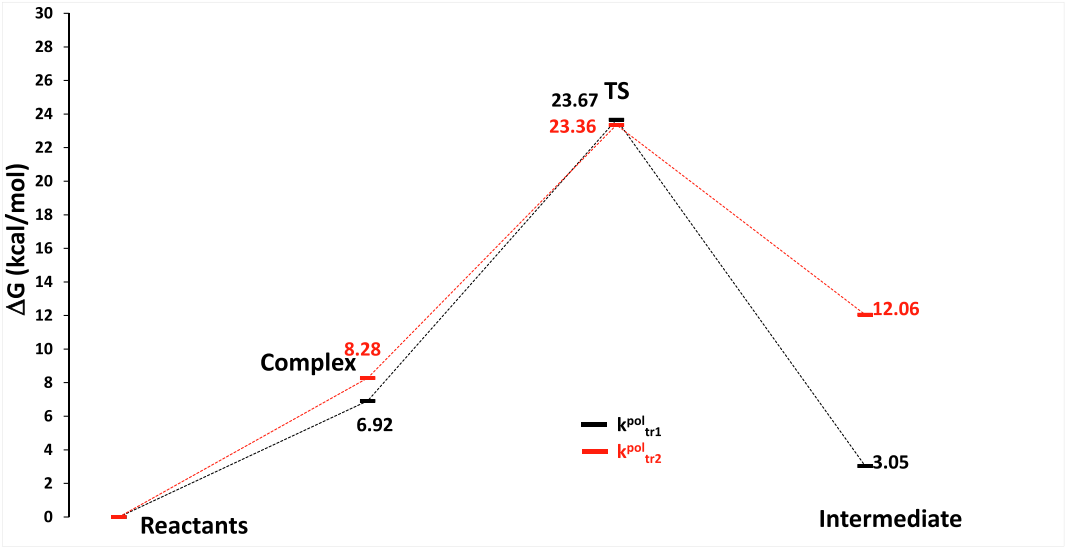

b) 2-EHA

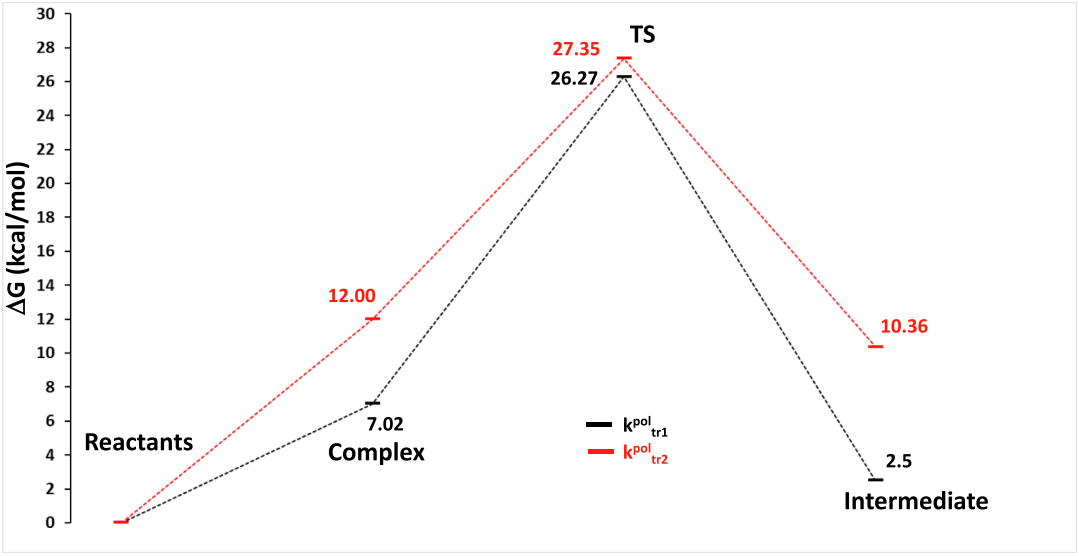

Fig. 3. Potential energy surface for the hydrogen abstraction in intermolecular chain transfer to polymer reactions: a) 2-OA b) 2-EHA. k_{tr1}^{pol} is the rate coefficient of the hydrogen abstraction from polymer backbone and k_{tr2}^{pol} is the rate coefficient of the hydrogen abstraction from the side chain. Calculated at the M062X/6-311++G (2df,2p)//M062X/6-31+G(d) level of theory.

through formation of a complex which is less stable than the reactants in both cases. The reactions then go through a transition state which is shown to be more energetic in Gibbs free energy for the hydrogen abstraction from the hydrogen in the double bond (37.59 kcal/mol and 28.80 kcal/mol for k_{tr1}^{mon} and k_{tr2}^{mon}, respectively), and also the forming intermediate is less stable. The electronic barrier for k_{tr1}^{mon} is calculated as $\Delta E_0 = 18.85$ kcal/mol (78.86 kJ/mol) which is much higher than the value calculated for k_{tr2}^{mon} $\Delta E_0 = 12.43$ kcal/mol (46.5 kJ/mol). It can be concluded that the chain transfer to monomer reaction mainly goes through the reaction path of abstraction of the hydrogen from the side chain at moderate reaction temperatures.

As it was mentioned before, higher degree of branching was observed experimentally for 2-EHA [14]. This experimental finding can have the origin on the higher backbiting rate coefficient of 2-EHA compared to 2-OA (see Figure S.7 for the reaction mechanism of backbiting for 2-OA and 2-EHA homopolymers). To shed light on this, the electronic barrier of the backbiting reaction was calculated by DFT which led to very similar values, $\Delta E0 = 65.6$ kJ/mol and $\Delta E0 = 63.3$ kJ/mol for 2-OA and 2-EHA, respectively. The potential surface energy (shown in Figure S.6, **section S.5**) also shows very similar Gibbs free energy barrier of the transition states for both monomers leading to stable intermediates, which indicates very similar backbiting rate coefficient for both 2-EHA and 2-OA monomers.

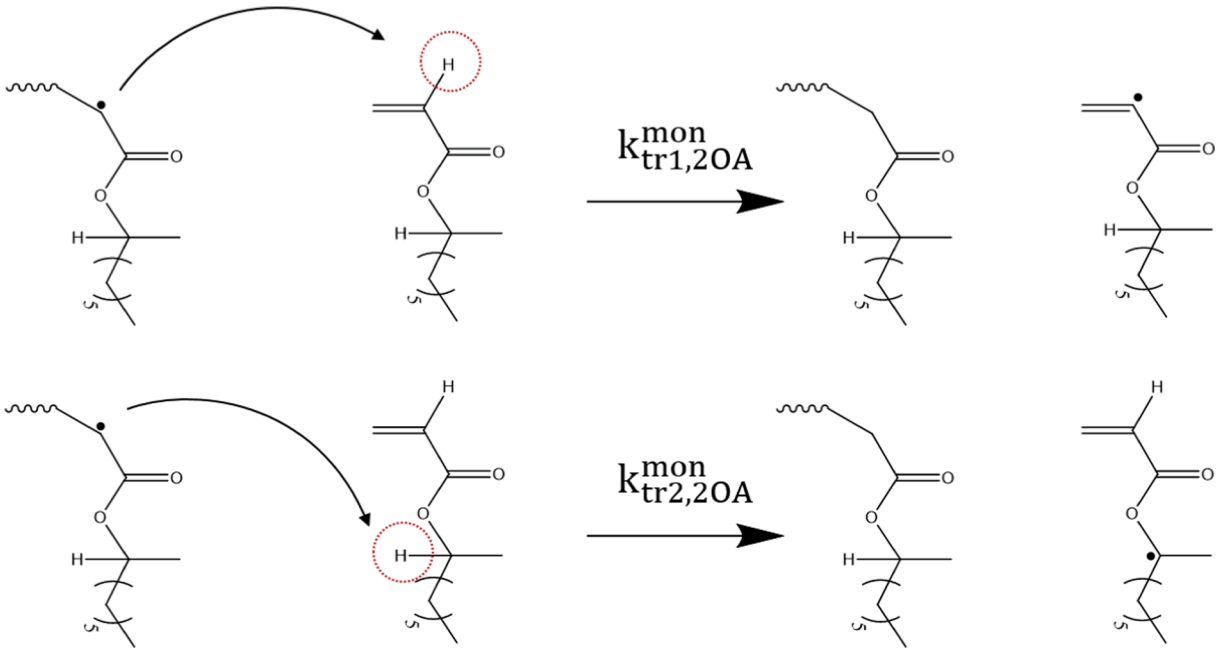

Fig. 4. Possible reaction mechanisms for chain transfer to monomer reaction in homopolymerizations of 2-OA.

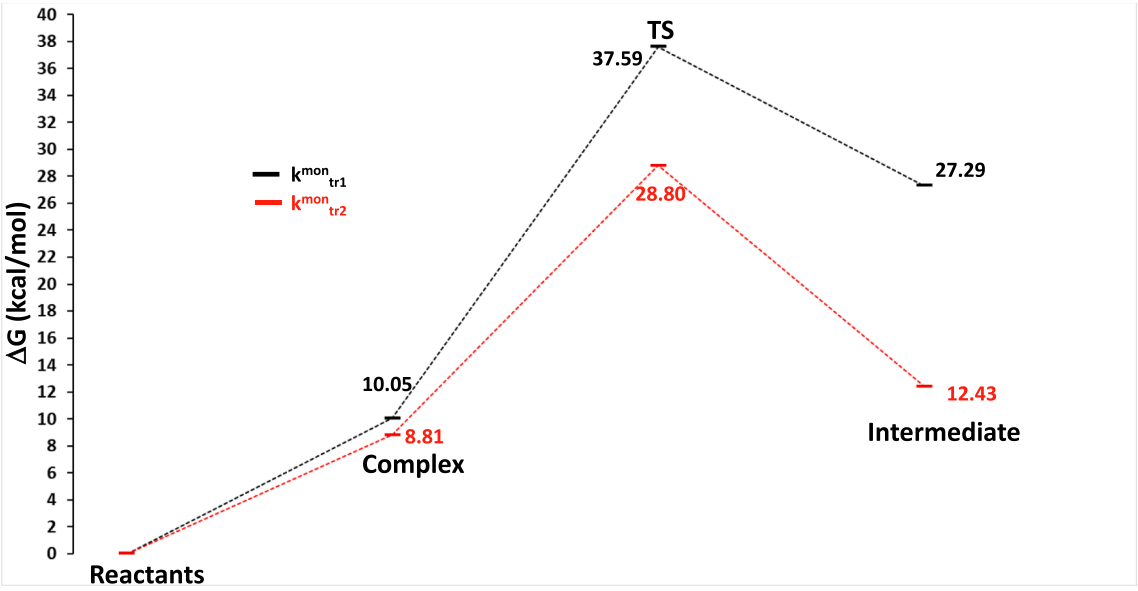

Fig. 5. Potential energy surface for the hydrogen abstraction in chain transfer to monomer reactions of 2-OA. k_{tr1}^{mon} is the rate coefficient of the hydrogen abstraction from double bond hydrogen and k_{tr2}^{mon} is the rate coefficient of the hydrogen abstraction from the side chain. Calculated at the M062X/6-311++G(2df,2p)//M062X/6-31+G(d) level of theory.

5.2. Kinetic Monte Carlo modelling

In light of the ratio between two possible intermolecular chain transfer to polymer rate coefficients given by the quantum chemistry calculations for the 2-EHA and 2-OA homopolymerizations, the two systems were simulated using the Monte Carlo model described above. The full kinetic schemes and kinetic rate coefficients considered for both monomer systems are described in the Supporting Information (Scheme S.1, Table S.2, section S.3). Briefly, initiation, propagation, termination and secondary reactions of the acrylates, namely, backbiting and intermolecular chain transfer to polymer were considered in the model. As the reactions were performed at moderate temperature (70 °C), β-scission, and as a result, the production of macromonomers which are more relevant at elevated temperatures [42,43], were neglected in the model. The rate of radical absorption was considered to be proportional to the radius of the particles ($k_a = r_p \times k_a^*$) and the desorption rate coefficient was considered proportional to the inverse of the second power of the radius of the particle ($k_d = r_p^{-2} \times k_d^*$) [25]. As the absorption and desorption rate coefficients are highly correlated, the desorption rate parameter (k_d^*) was considered equal to the value reported for the homopolymerization of butyl acrylate [44] and the absorption coefficient was adjusted to fit the polymerization kinetics. A monodisperse particle size distribution of the polystyrene seed with $d_p = 81$ nm was considered in the model.

Being a relatively new monomer, there is a complete lack of kinetic data for 2-OA. Even the propagation rate coefficient of the secondary

radical, the most common kinetic parameter, is not reported to the authors' best of knowledge. Even more, and despite its wide industrial use, there is also a notable lack of kinetic parameter data regarding the 2-ethylhexyl acrylate, especially at high temperature. This is mainly due to the inherent experimental difficulties associated with the side reactions that are characteristic of acrylates. Namely, intramolecular chain transfer (backbiting) reactions affects both the rate of polymerization and polymer molar mass distribution, and can induce errors when the rate coefficient is measured by pulsed laser polymerization-size exclusion chromatography technique (PLP-SEC). To reduce the effect of backbiting reaction on the measurement of propagation rate coefficient of the secondary radicals, Junkers *et al.* used high frequency PLP-SEC to measure the most accurate propagation rate coefficient of the secondary radicals to date for 2-EHA, $k_p = 9.1 \times 10^6 \exp(15.8/RT)$ [45], 3.85×10^4 $Lmol^{-1}s^{-1}$ at 70 °C. Other kinetic parameters such as the backbiting rate coefficient (k_{bb}) are even more challenging to measure. Lena *et al.* used electrospray-ionization (ESI) mass spectrometry (MS) combined with ^{13}C NMR to estimate k_{bb} reporting $4.46 \times 10^8 \exp(-35.9/RT)$, 1535 s^{-1} at 70 °C[46]. On the other hand, Quintens *et al.* used PLP-SEC data to estimate $k_{bb} = 1.46 \times 10^7 \exp(-32.2/RT)$, 183 s^{-1} at 70 °C [47] by fitting the apparent k_p in a PLP-SEC experiment. As can be seen, there is a significant scatter in the data that can be obtained on the rate coefficient of the backbiting reaction, with constants that differ in an order of magnitude. On the other hand, the data available in the literature for the propagation rate coefficient of the tertiary radicals was estimated in a work combining PLP-SEC data and a model, using a correlation between average apparent propagation rate coefficient, backbiting and propagation rate coefficient of secondary and tertiary radicals [47].

Herein, the propagation rate coefficient of the secondary radicals of 2-EHA determined via high frequency (500 Hz) PLP-SEC available in the literature was used for both monomer systems [45]. Due to high correlation of k_{bb} and k_p^{ter}, they typically need simultaneous determination. In this work, the k_p^{ter} was set as the value corresponding to the n-butyl acrylate and backbiting parameter was used as an adjusting parameter to fit the final branching density of the polymer. Chain transfer to monomer rate coefficient of n-BA was used for 2-EHA [41] and also for 2-OA as in the DFT calculations, it was shown that one of the chain transfer to monomer reaction routes is less favoured to occur. Therefore, it was assumed that the overall rate coefficient is not affected by the presence of two abstractable hydrogens in 2-OA. Termination rate coefficients of secondary and tertiary radicals corresponding to n-BA were used in the model.

The absorption parameter (k_a^*) together with the backbiting (k_{bb}) and the overall intermolecular chain transfer to polymer ($k_{tr1}^{pol} + k_{tr2}^{pol}$) were used as fitting parameters for 2-EHA homopolymerization. The rate coefficients of intermolecular chain transfer to polymer from the backbone (k_{tr1}^{pol}), and the side chain (k_{tr2}^{pol}) were later calculated using the overall estimated intermolecular chain transfer to polymer and the ratio between the coefficients obtained in the DFT calculations. The above-mentioned adjusting parameters were used to fit the experimental data on instantaneous conversion, final branching density, the evolution of the molar mass distribution (MMD) and gel content. In the case of 2-OA, due to the similarity on the monomer structure, adjusted absorption parameter for 2-EHA were considered also for 2-OA homopolymerization. In addition, in light of the DFT results which showed very similar activation energies and potential surface energy of the backbiting of both monomer systems, the adjusted backbiting constant for 2-EHA was used in the 2-OA homopolymerizations model despite the differences seen in the final experimental branching density. As a result only one parameter was adjusted in case of 2-OA homopolymerizations, i.e. overall intermolecular chain transfer to polymer. Using this estimated value and the ratio between the coefficients obtained in the DFT calculations, the rate coefficients of intermolecular chain transfer to polymer from the backbone (k_{tr1}^{pol}) and the side chain (k_{tr2}^{pol}) were calculated.

In summary, considering all the unknown parameters and uncertainties on the kinetic parameters in both monomer homopolymerization systems, herein we tried to reduce the number of the unknown parameters by using these parameters from BA homopolymerization and estimate only the most sensitive parameters to fit the gathered experimental data on the microstructure; mainly the branching density, MMD and the gel content.

Figs. 6 and 7 show the comparison of the model prediction and the experimental results of the homopolymerizations of 2-EHA and 2-OA for the evolution of monomer conversion, particle size, branching density, evolution of MMD and gel content. The adjusting parameters used in the model are reported in Table 1.

The model predicts reasonably well the kinetics of the polymerization of 2-EHA and the final branching density. Due to high instantaneous conversion of the experiments, the branching density shows high values from the beginning of the reaction and increases slightly during the reaction. The estimated value for the k_{bb} of 2-EHA is 525.5 s^{-1} at 70 °C which is in between the two reported values of k_{bb}: $1.46 \times 10^7 \exp(-32.2/RT)$ [47], 183 s^{-1} at 70 °C and $4.46 \times 10^8 \exp(-35.9/RT)$, 1530 s^{-1} at 70 °C [46]. The first one was estimated for this monomer by fitting the apparent k_p in a PLP-SEC experiment. It is worth mentioning that no data on branching level was used in the estimation of this parameter due to inherent experimental limitation of measuring branching level at very low polymer concentration. The estimated value is comparable to the n-BA reported rate coefficients of backbiting at the same temperature ($7.41 \times 10^7 \exp(-32.7/RT)$ [48], 779 s^{-1} at 70 °C and $3.2 \times 10^{10} \exp(-52.3/RT)$ [49], 349 s^{-1} at 70 °C).

Fig. 6**c** shows the evolution of the MMD measured by AF4/MALS/RI. It can be seen that from early hour of the reaction a bimodal distribution has been formed with a population at high molar masses that corresponds to the gel fraction. This population moves to higher molar masses through the reaction, i.e. increasing the gel fraction and corresponding MM. The model predicts well the trend in the evolution of the molar mass distribution showing a completely bimodal distribution; each mode corresponding to sol and gel fractions, respectively (Fig. 6**d**). In the model, the high molar mass mode of the full molar mass distribution is considered as gel, which is equivalent to considering polymer chains with molar mass higher than 10^8 g/mol as gel. The gel content experimentally was measured by two methods: Soxhlet extraction and by using the refractive index signal after fractionation in the AF4/MALS/RI (see Supporting Information section S.2). The comparison in Fig. 6**e** shows that the gel fraction obtained from the RI signal after fractionation of the sample in the AF4 shows higher gel contents than the Soxhlet data with a significant difference at the beginning of the reaction, however, this discrepancy reduces through the reaction and the final gel fraction measured by both methods are close. It is worth mentioning that the gel fraction measurement in Soxhlet is based on the solubility of the polymer in THF. At the beginning of the reaction, although the high molar mass mode has been formed and can be seen in the AF4/MALS/RI MMD, part of this population can be soluble. Along the reaction the gel molar mass increases and this population becomes more and more insoluble and therefore the AF4/MALS/RI and Soxhlet measurements of the gel fraction become closer. The gel fraction predicted by the model, shows high fraction of the gel from early hour of the reaction and evolves slowly during the reaction. The fraction of the gel from 2 h on and the final gel content fits very well with both experimental gel fractions. This discrepancy on the predicted gel fraction at the beginning of the reaction in the seeded semibatch emulsion polymerization of 2-EHA has been reported before.[41].

Fig. 7**a and 7b** show the comparison of the evolution of the instantaneous conversion, particle size and branching density for 2-OA homopolymerization. The model fits well the kinetics of the reaction while higher branching density is predicted. It is worth recalling here that in light of the DFT calculations, the same rate coefficient of backbiting was used in the model (that estimated for 2-EHA), although lower experimental branching density of the final sample for 2-OA (measured

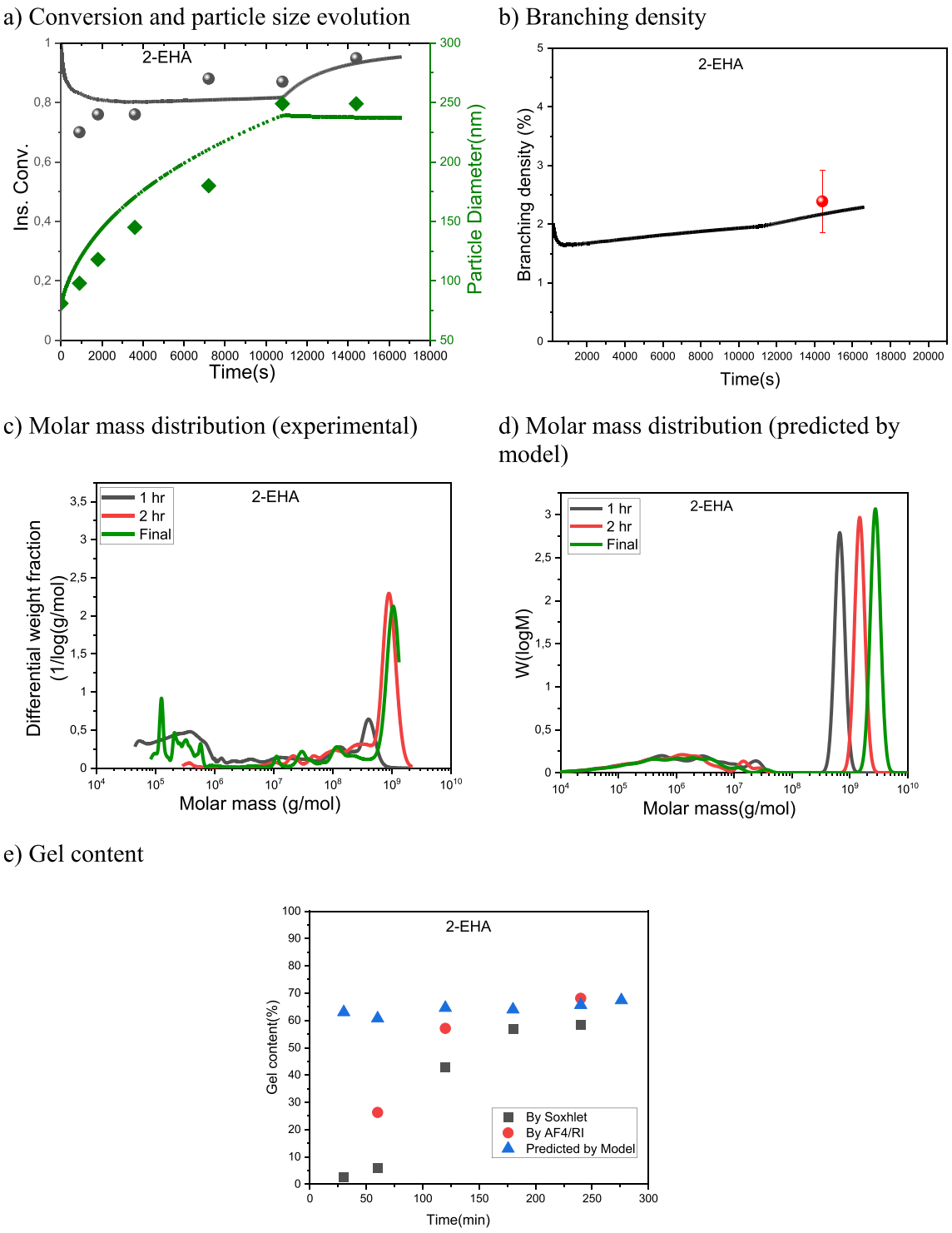

Fig. 6. Comparison of the model prediction and the experimental results of the homopolymerizations of 2-EHA a) monomer instantaneous conversion and particle size; b) branching density; c) experimental evolution of MMD by AF4/MALS/RI; d) predicted evolution of MMD by Monte Carlo simulation; e) evolution of the gel content.

at final conversion of 94.1 %) was reported in reference 14 compared to the one for 2-EHA (measured at final conversion of 94.9 %). Lovell et al. [50] studied the branching density of a series of alkyl acrylates in semi-batch emulsion homopolymerizations. The acrylate polymers with non-linear side-groups showed clearly higher branching level compared to the n-alkyl acrylate homopolymers. It is shown that 2-EHA and *iso*-octyl acrylate homopolymers showed higher branching density compared to the n-octyl acrylate homopolymer. However, no significant difference was reported between non-linear isomers; i.e., 2-EHA and *iso*-octyl. This data confirms finding of the DFT calculations.

The evolution of MMD measured by AF4/MALS/RI and predicted by model are shown in Fig. 7**c and 7d**. Bimodal distributions that increase the molar mass and amount of the high molar mass mode are also observed for 2-OA. Comparing with the 2-EHA, the gel population has higher molar mass and the gel fraction is higher. These microstructural differences are very well captured by the model, i.e. predicting higher

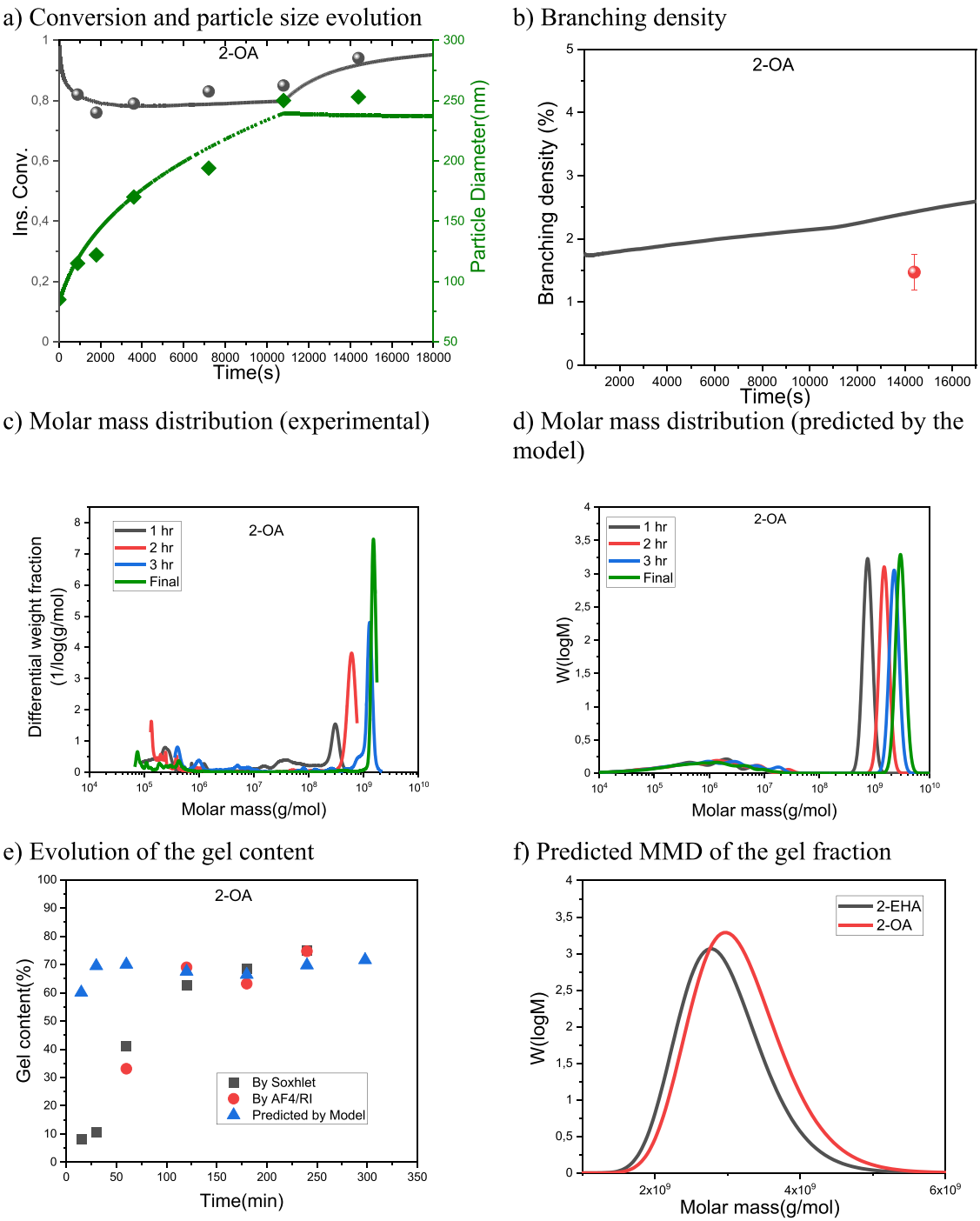

Fig. 7. Comparison of the model prediction and the experimental results of the polymerizations of 2-OA a) monomer instantaneous conversion and particle size; b) branching density; c) experimental evolution of MMD by AF4/MALS/RI; d) predicted evolution of MMD by Monte Carlo simulation; e) evolution of the gel content; f) comparison of the predicted MMD of the gel in the final sample of 2-EHA and 2-OA polymers.

Table 1
Adjusted parameters used in the model in the homopolymerization of 2-OA or 2-EHA at 70 °C.

Parameter	Adjusted value	
	2-EHA	2-OA
$k_{bb}(s^{-1})$	525.5	525.5
$k_{tr1}^{pol}(Lmol^{-1}s^{-1})$	63.34	54.84
$k_{tr2}^{pol}(Lmol^{-1}s^{-1})$	11.90	80.06
$k_a^*(s^{-1}dm^{-1})$	1.1×10^7	1.1×10^7

percentage of gel (Fig. 7**e**) as well as higher molar mass of the gel population (Fig. 7**f**) for 2-OA compared to 2-EHA. Similar to the case of 2-EHA, the evolution of the gel fraction is well captured after 2 h of the reaction compared to both experimental results. The calculated value for the k_{tr1}^{pol} (using the estimated rate coefficient for the overall intermolecular chain transfer to polymer and the ratios of $k_{tr1}^{pol}/k_{tr2}^{pol}$ obtained by the DFT simulations), shows slightly higher values for 2-EHA 63.34 $(Lmol^{-1}s^{-1})$ compared to 54.84 $(Lmol^{-1}s^{-1})$ for 2-OA, however it can be seen that the main difference lies on the values of intermolecular chain transfer coefficient from the side chain, k_{tr2}^{pol}, which was estimated to be

higher in the case of 2-OA.

6. Conclusions

The origin of the previously reported differences on the microstructure of bio-based and oil-based C8 alkyl polyacrylates synthesized by emulsion polymerization was assessed by a combined mathematical model effort. The emulsion polymerization process was simulated by a Monte Carlo model that includes mechanisms of intramolecular chain transfer (backbiting), intermolecular chain transfer to polymer (considering the transfer in both backbone and side chain labile hydrogens) as well as chain transfer to monomer that were analyzed in detail by DFT calculations, to shed light on the differences of the kinetic rate coefficients for both monomers (i.e. 2-OA and 2-EHA).

2-EHA and 2-OA homopolymers synthesized by seeded semibatch emulsion polymerization were studied in this work. These monomers both possess two labile hydrogens. DFT calculations showed that the hydrogen in the side chains of 2-OA is more labile than the backbone hydrogen ($\frac{k_{tr1}^{pol}}{k_{tr2}^{pol}} = 0.68$), while completely different trend was calculated for 2-EHA ($\frac{k_{tr1}^{pol}}{k_{tr2}^{pol}} = 5.32$). It was found that the activation energies of both intermolecular chain transfer to polymer reactions are higher in 2-EHA than in 2-OA resulting in higher overall rate coefficient of intermolecular chain transfer to polymer for 2-OA than for 2-EHA. In addition, the chain transfer to monomer via hydrogen abstraction of both labile hydrogens in the monomer was studied. It was found that the activation energy of chain transfer to monomer of 2-OA on the monomer side chain (k_{tr2}^{mon}) is comparable to the one for the n-butyl acrylate while k_{tr1}^{mon} showed very high activation energy, concluding that the chain transfer to monomer reactions mainly go through the reaction path of abstraction of the hydrogen from the monomer side chain. Despite the differences observed experimentally in the branching density of the 2-EHA and 2-OA, the DFT calculation showed very similar barrier of the transition states in Gibbs free energy and similar activation energies for both monomer systems.

In light of the findings of the DFT calculations, a kinetic Monte Carlo model was used to predict the kinetics and microstructure of the homopolymers of 2-EHA and 2-OA. The rate coefficients of the backbiting, overall intermolecular chain transfer to polymer and radical absorptions coefficients were considered as adjusting parameters in the model. In both polymerization systems, the model was able to fit well both kinetics and microstructure properties including the branching density, evolution of the MMD and the gel content and also the microstructural differences between two systems, namely; higher amount of gel and molar mass of the gel. It was demonstrated that the microstructural differences on gel fraction and MMD lies on the different overall values of intermolecular chain transfer coefficient for homopolymers under study. This difference mainly originated from the different contributions of the chain transfer to polymer from the side chain, k_{tr2}^{pol}, which is shown to be higher in 2-OA (80.06 $Lmol^{-1}s^{-1}$), compared to 2-EHA (11.90 $Lmol^{-1}s^{-1}$). The estimated value of backbiting reaction rate coefficient of 2-EHA and 2-OA is in the range of the scattered values reported for 2-EHA monomer.

CRediT authorship contribution statement

Shaghayegh Hamzehlou: Conceptualization, Methodology, Software, Writing – original draft. **Aitor Barquero:** Conceptualization, Methodology, Investigation, Writing – original draft. **Amaia Agirre:** Investigation. **Fernando Ruipérez:** Software, Writing – review & editing. **Jose Ramon Leiza:** Conceptualization, Methodology, Writing – review & editing.

Declaration of Competing Interest

The authors declare that they have no known competing financial interests or personal relationships that could have appeared to influence the work reported in this paper.

Data availability

Data will be made available on request.

Acknowledgements

The authors would like to thank the financial support received from the Basque Government (IT-1525-22), from the Spanish Government (MINECO PID2021-123146OB-I00, MICINN PDC2021-121416-I00 and PID-117628RJ-I00)).

Appendix A. Supplementary material

Supplementary data to this article can be found online at https://doi.org/10.1016/j.eurpolymj.2023.112410.

References

[1] M. Aguirre, N. Ballard, E. Gonzalez, S. Hamzehlou, H. Sardon, M. Calderon, M. Paulis, R. Tomovska, D. Dupin, R.H. Bean, T.E. Long, J.R. Leiza, J.M. Asua, Polymer colloids: current challenges, emerging applications, and new developments, Macromolecules 56 (2023) 2579–2607, https://doi.org/10.1021/acs.macromol.3c00108.

[2] S. Molina-Gutiérrez, V. Ladmiral, R. Bongiovanni, S. Caillol, P. Lacroix-Desmazes, Radical polymerization of biobased monomers in aqueous dispersed media, Green Chem. 21 (2019) 36–53, https://doi.org/10.1039/c8gc02277a.

[3] A. Parodi, A. Jorea, M. Fagnoni, D. Ravelli, C. Samorì, C. Torri, P. Galletti, Bio-based crotonic acid from polyhydroxybutyrate: synthesis and photocatalyzed hydroacylation, Green Chem. 23 (2021) 3420–3427, https://doi.org/10.1039/d1gc00421b.

[4] A.I. Magalhães, J.C. de Carvalho, J.D.C. Medina, C.R. Soccol, Downstream process development in biotechnological itaconic acid manufacturing, Appl. Microbiol. Biotechnol. 101 (1) (2017) 1–12.

[5] J. Sebastian, C. Osorio-Gonzalez, T. Rouissi, K. Hegde, S.K. Brar, Bioderived fumaric acid for sustainable production of key active pharmaceutical ingredients: dimethyl fumarate and Monomethyl fumarate, Process Biochem. 120 (2022) 35–40, https://doi.org/10.1016/j.procbio.2022.05.017.

[6] T. Nabuurs, On the road to a more natural finish, Eur. Coatings J. 4 (2018) 20–24.

[7] H. Fouilloux, W. Qiang, C. Robert, V. Placet, C.M. Thomas, Multicatalytic transformation of (meth)acrylic acids: a one-pot approach to biobased poly(meth) acrylates, Angew. Chemie - Int. Ed. 60 (2021) 19374–19382, https://doi.org/10.1002/anie.202106640.

[8] J.G.H. Hermens, A. Jensma, B.L. Feringa, Highly efficient biobased synthesis of acrylic acid, Angew. Chemie - Int. Ed. 61 (2022) 1–6, https://doi.org/10.1002/anie.202112618.

[9] A. Badía, J. Movellan, M.J. Barandiaran, J.R. Leiza, High biobased content latexes for development of sustainable pressure sensitive adhesives, Ind. Eng. Chem. Res. 57 (2018) 14509–14516, https://doi.org/10.1021/acs.iecr.8b03354.

[10] A. Badía, A. Agirre, M.J. Barandiaran, J.R. Leiza, Easy removable and UV tunable biobased waterborne pressure sensitive adhesives, Int. J. Adhes. Adhes. 108 (2021), https://doi.org/10.1016/j.ijadhadh.2021.102860.

[11] E. González, R. Stuhr, J.M. Vega, E. García-lecina, H.J. Grande, J.R. Leiza, M. Paulis, Assessing the effect of CeO2 nanoparticles as corrosion inhibitor in hybrid biobased waterborne acrylic direct to metal coating binders, Polymers (Basel). 13 (2021), https://doi.org/10.3390/polym13060848.

[12] A. Riondel, C. Graire, M. Esch, R. Linemann, Industrial process for manufacture of 2-octyl acrylate by transesterification with high purity and output, WO 2013110876 (2013) A1.

[13] J.L. Colby, T.A. Clem, T.D. Spawn, A.E. Hutt, W.T. Teply, Selective synthesis of 2-octyl acrylate by acid catalyzed esterification of 2-octanol and acrylic acid, US 20160002140 (2016) A1.

[14] M. Barrenetxe, A. Agirre, J.I. Santos, A. Badía, J.R. Leiza, A. Barquero, Oil-based vs Bio-Based C8 Alkyl Chain (Meth)Acrylates in Emulsion Polymerization: Kinetics and Microstructure, Macromol. React. Eng. (2022).

[15] C. Plessis, G. Arzamendi, J.R. Leiza, H.A.S. Schoonbrood, D. Charmot, J.M. Asua, A Decrease in effective acrylate propagation rate constants caused by intramolecular chain transfer, Macromolecules 33 (2000) 4–7, https://doi.org/10.1021/ma991205z.

[16] C. Plessis, G. Arzamendi, J.R. Leiza, H.A.S. Schoonbrood, D. Charmot, J.M. Asua, Seeded semibatch emulsion polymerization of n -butyl acrylate, Kinet. Struct. Propert. Macromol. 33 (14) (2000) 5041–5047.

[17] N.M. Ahmad, F. Heatley, P.A. Lovell, Chain transfer to polymer in free-radical solution polymerization of n -butyl acrylate studied by NMR spectroscopy, Macromolecules 31 (9) (1998) 2822–2827.
[18] A. Agirre, J.I. Santos, J.R. Leiza, Toward understanding the architecture (branching and MWD) of crosslinked acrylic latexes, Macromol. Chem. Phys. 214 (2013) 589–598, https://doi.org/10.1002/macp.201200482.
[19] P. Castignolles, R. Graf, M. Parkinson, M. Wilhelm, M. Gaborieau, Detection and quantification of branching in polyacrylates by size-exclusion chromatography (SEC) and melt-state 13C NMR spectroscopy, Polymer (Guildf). 50 (2009) 2373–2383, https://doi.org/10.1016/j.polymer.2009.03.021.
[20] D. Britton, F. Heatley, P.A. Lovell, Chain transfer to polymer in free-radical bulk and emulsion polymerization of vinyl acetate studied by NMR spectroscopy, Macromolecules 31 (1998) 2828–2837, https://doi.org/10.1021/ma971284j.
[21] H. Tobita, Monte Carlo simulation of emulsion polymerization-linear, branched, and crosslinked polymers, Acta Polym. 46 (1995) 185–203.
[22] E. Jabbari, Monte Carlo simulation of tri-functional branching and tetra-functional crosslinking in emulsion polymerization of butadiene, Polymer (Guildf). 42 (2001) 4873–4884, https://doi.org/10.1016/S0032-3861(00)00880-6.
[23] G. Arzamendi, J.R. Leiza, Molecular weight distribution (soluble and insoluble fraction) in emulsion polymerization of acrylate monomers by monte carlo simulations, Ind. Eng. Chem. Res. 47 (2008) 5934–5947, https://doi.org/10.1021/ie701752f.
[24] J.A. Rawlston, J. Guo, F.J. Schork, M.A. Grover, A kinetic Monte Carlo study on the nucleation mechanisms of oil-soluble initiators in the miniemulsion polymerization of styrene, J. Polym. Sci. A Polym. Chem. 46 (2008) 6114–6128, https://doi.org/10.1002/pola.
[25] S. Hamzehlou, Y. Reyes, J.R. Leiza, Modeling the mini-emulsion copolymerization of N-butyl acrylate with a water-soluble monomer: a Monte Carlo approach, Ind. Eng. Chem. Res. 53 (2014) 8996–9003, https://doi.org/10.1021/ie403182t.
[26] A.K. Tripathi, J.G. Tsavalas, Ghost-mirror approach for accurate and efficient kinetic monte carlo simulation of seeded emulsion polymerization, Macromol. Theory Simulations. 29 (2020) 2000033, https://doi.org/10.1002/mats.202000033.
[27] Y.W. Marien, P.H.M. Van Steenberge, R.D. Dagmar, G.B. Marin, Particle by particle kinetic monte carlo tracking of reaction and mass transfer events in miniemulsion free radical polymerization, Macromolecules 52 (2019) 1408–1423, https://doi.org/10.1021/acs.macromol.8b02508.
[28] D.T. Gillespie, Stochastic simulation of chemical kinetics, Annu. Rev. Phys. Chem. 58 (2007) 35–55, https://doi.org/10.1146/annurev.physchem.58.032806.104637.
[29] M. Zubitur, P.D. Armitage, S. Ben Amor, J.R. Leiza, J.M. Asua, Mathematical modeling of multimonomer (vinylic, Divinylic, Acidic) emulsion copolymerization systems, Polym. React. Eng. 11 (4) (2003) 627–662.
[30] E. Mavroudakis, K. Liang, D. Moscatelli, R.A. Hutchinson, A Combined computational and experimental study on the free-radical copolymerization of styrene and hydroxyethyl acrylate, Macromol. Chem. Phys. 213 (2012) 1706–1716, https://doi.org/10.1002/macp.201200165.
[31] D. Cuccato, E. Mavroudakis, D. Moscatelli, Quantum chemistry investigation of secondary reaction kinetics in acrylate-based copolymers, Chem. A Eur. J. 117 (21) (2013) 4358–4366.
[32] M.L. Coote, Quantum-chemical modeling of free-radical polymerization, Macromol. Theory Simulations. 18 (2009) 388–400, https://doi.org/10.1002/mats.200900050.
[33] M. Bandiera, S. Hamzehlou, F. Ruipérez, M. Aguirre, R. Balk, M.J. Barandiaran, J. R. Leiza, Copolymerization of (meth)acrylates with vinyl aromatic macromonomers: Understanding the mechanism of retardation on the kinetics with acrylates, Polym. Chem. 10 (2019) 1769–1779, https://doi.org/10.1039/c9py00062c.
[34] A. Simula, F. Ruipérez, N. Ballard, J.R. Leiza, S. Van Es, J.M. Asua, Why can Dispolreg 007 control the nitroxide mediated polymerization of methacrylates? Polym. Chem. 10 (2019) 106–113, https://doi.org/10.1039/c8py00900g.
[35] Y. Zhao, D.G. Truhlar, The M06 suite of density functionals for main group thermochemistry, thermochemical kinetics, noncovalent interactions, excited states, and transition elements: two new functionals and systematic testing of four M06-class functionals and 12 other function, Theor. Chem. Acc. 120 (2008) 215–241, https://doi.org/10.1007/s00214-007-0310-x.
[36] W.J. Hehre, R. Ditchfield, J.A. Pople, Self-Consistent Molecular Orbital Methods. XII. Further Extensions of Gaussian-Type Basis Sets for Use in Molecular Orbital Studies of Organic Molecules, J. Chem. Phys. 56 (1972) 2257–2261. 10.1063/1.1677527.
[37] R. Krishnan, J.S. Binkley, R. Seeger, J.A. Pople, Self-consistent molecular orbital methods. XX. A basis set for correlated wave functions, J. Chem. Phys. 72 (1980) 650–654. 10.1063/1.438955.
[38] D.J. Frisch, M. J.; Trucks, G. W.; Schlegel, H. B.; Scuseria, G. E.; Robb, M. A.; Cheeseman, J. R.; Scalmani, G.; Barone, V.; Mennucci, B.; Petersson, G. A.; Nakatsuji, H.; Caricato, M.; Li, X.; Hratchian, H. P.; Izmaylov, A. F.; Bloino, J.; Zheng, G.; Sonnenb, Gaussian 09 Revision A.1, (2009).
[39] F. Ruipérez, Application of quantum chemical methods in polymer chemistry, Int. Rev. Phys. Chem. 38 (2019) 343–403, https://doi.org/10.1080/0144235X.2019.1677062.
[40] B.B. Noble, M.L. Coote, First principles modelling of free-radical polymerisation kinetics, Int. Rev. Phys. Chem. 32 (2013) 467–513, https://doi.org/10.1080/0144235X.2013.797277.
[41] C. Plessis, G. Arzamendi, J.M. Alberdi, M. Agnely, J.R. Leiza, J.M. Asua, Intramolecular chain transfer to polymer in the emulsion polymerization of 2-ethylhexyl acrylate, Macromolecules 34 (17) (2001) 6138–6143.
[42] M. Edeleva, Y.W. Marien, P.H.M.V.S. Streenberge, D.R. Ďhooge,, Impact of side reactions on molar mass distribution, unsaturation level and branching density in solution free radical polymerization of n-butyl acrylate under well-defined lab-scale reactor conditions, Polym. Chem. 12 (2021) 2095–2114, https://doi.org/10.1039/d1py00151e.
[43] J. Chiefari, J. Jeffery, R.T.A. Mayadunne, G. Moad, E. Rizzardo, S.H. Thang, Chain transfer to polymer: a convenient route to macromonomers, Macromolecules 32 (1999) 7700–7702, https://doi.org/10.1021/ma990488s.
[44] N. Ballard, S. Hamzehlou, F. Ruipérez, J.M. Asua, On the termination mechanism in the radical polymerization of acrylates, (2016) 1–5. 10.1002/marc.201600278.
[45] T. Junkers, M. Schneider-Baumann, S.S.P. Koo, P. Castignolles, C. Barner-Kowollik, Determination of propagation rate coefficients for methyl and 2-ethylhexyl acrylate via high frequency PLP−SEC under consideration of the impact of chain branching, Macromolecules 43 (2010) 10427–10434, https://doi.org/10.1021/ma102130h.
[46] J.-B. Lena, M. Deschamps, N.F. Sciortino, S.L. Masters, M.A. Squire, G.T. Russell, Effects of chain transfer agent and temperature on branching and β-scission in radical polymerization of 2-ethylhexyl acrylate, Macromol. Chem. Phys. 1700579 (2018) 1700579, https://doi.org/10.1002/macp.201700579.
[47] G. Quintens, T. Junkers, Pulsed laser polymerization-size exclusion chromatography investigations into backbiting in ethylhexyl acrylate polymerization, Polym. Chem. 13 (2022) 2019–2025, https://doi.org/10.1039/d1py01533h.
[48] A.N. Nikitin, R.A. Hutchinson, G.A. Kalfas, J.R. Richards, C. Bruni, The effect of intramolecular transfer to polymer on stationary free-radical polymerization of alkyl acrylates, 3 - consideration of solution polymerization up to high conversions, Macromol. Theory Simulations. 18 (2009) 247–258, https://doi.org/10.1002/mats.200900009.
[49] S. Hamzehlou, N. Ballard, Y. Reyes, A. Aguirre, J.M. Asua, J.R. Leiza, Analyzing the discrepancies in the activation energies of the backbiting and β-scission reactions in the radical polymerization of n-butyl acrylate, Polym. Chem. 7 (2016) 2069–2077, https://doi.org/10.1039/C5PY01990G.
[50] I. Gray, F. Heatley, P.A. Lovell, Effect of side-group structure and temperature on chain transfer to polymer and branching in acrylate homopolymerizations, Colloid Polym. Sci. 300 (2022) 445–463, https://doi.org/10.1007/s00396-021-04935-1.